

NONLINEAR STELLAR PULSATION

Editors: M. Takeuti & D. Sasselov

in Astrophysics and Space Science Library (ASSL)

Chapter 1

NONLINEAR ANALYSIS OF IRREGULAR VARIABLES

J. Robert Buchler

Physics Department, University of Florida

Gainesville FL32611, USA

buchler@physics.ufl.edu

Zoltán Kolláth

Konkoly Observatory

P.O. Box 67, H-1525 Budapest, Hungary

kollath@konkoly.hu

Abstract The Fourier spectral techniques that are common in Astronomy for analyzing periodic or multi-periodic light-curves lose their usefulness when they are applied to unsteady light-curves. We review some of the novel techniques that have been developed for analyzing irregular stellar light or radial velocity variations, and we describe what useful physical and astronomical information can be gained from their use.

Keywords: Variable stars, Semi-Regular stars, W Virginis stars, Phase-space reconstruction, Nonlinear systems, Chaos, Fractal dimension, Time-frequency analysis, Topological analysis

1. INTRODUCTION

Is it possible, from the measurement of an irregular light-curve, to infer something interesting and physically useful about the mechanism that generated it? This is the fundamental question that we address in this review paper.

The first thing that comes to mind when confronted with a time-series is to perform a Fourier spectral analysis. Such an analysis

2 NONLINEAR STELLAR PULSATION

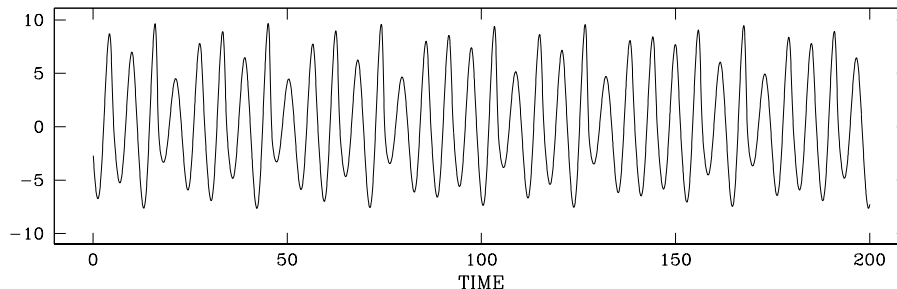


Figure 1.1 Temporal behavior of variable $x_1(t)$ of the Rössler oscillator.

is of course extremely useful when the signal is periodic or multi-periodic, but these two types of signals do not exhaust all possibilities. Signals can also be stochastic or chaotic, in which case the spectral analysis is not particularly insightful. (For a good general discussion of why the Fourier analysis or any other linear analyses such as ARMA break down *c.f.* Weigend & Gershenfeld, 1994 and Abarbanel *et al.* 1993).

As an example and a challenge to the astronomer reader we present the time-series shown in Fig. 1.1. The time-series shows large amplitude variations, yet according to the Fourier spectrum in Fig. 1.2, the signal appears to be mono-periodic. An O-C (observed-calculated) diagram displays phase meanderings. So what is the nature of this signal? In anticipation we note that this signal is the solution of a *deterministic* third order ordinary differential equation. It never repeats itself despite the apparent mono-periodic spectrum. In the nonlinear dynamics parlance this signal falls into the class of low dimensional chaos.

The signal that we have just discussed is a paradigm for understanding certain quite common types of real observational signals (even though of course the latter will in addition be contaminated by noise). We shall now describe in very simple terms three complementary techniques that we have found useful for analyzing such signals, namely an explicit functional reconstruction of the dynamics (sometimes referred to as global flow reconstruction), a topological analysis and a time-frequency analysis. References to technical details can be found in the cited references.

We have already presented a didactic review of the global flow reconstruction method (Varennia Lecture Notes, Buchler 1997) and there is no point in repetition. We therefore introduce the method slightly differently here in §2, and we emphasize the astrophysical results and applicability.

Can one always hope to extract information from a time-dependent signal about the physical system that has generated this signal? The answer is clearly no. First of all this would be hard if not impossible when the system is nonautonomous (*i.e.* the system itself changes on the time-scale of the signal). Second, it would be impractical when the number of degrees of freedom is neither large nor small. In the extremes of a large number of degrees of freedom (high dimensional phase-space) stochastic methods can be fruitfully applied, whereas in the case of a small number of degrees of freedom (low dimensional phase-space) the techniques from chaos theory apply. This is this latter type of system that we are concerned with here.

In §3 we briefly describe the Rössler system, a set of three first order equations, which displays a behavior (Fig. 1.1) that is still not very commonly known or understood in the astronomical community, but is a paradigm for certain types of irregular variable stars. As we have seen this system undergoes oscillations which appear almost mono-periodic in a Fourier spectrum, yet undergo wild oscillations in amplitude. An observational signal with this Fourier spectrum would almost certainly be classified as periodic.

2. FLOW RECONSTRUCTION

The basic idea that underlies the analysis that we are about to describe is really extremely simple. We illustrate it with the help of an example that is quite familiar to everybody, namely a second order differential equation with constant coefficients, or equivalently a system of two first order ode's, called a *two-dimensional flow*.

$$\frac{dy}{dt} = f(y) \tag{1.1}$$

where $y = (y_1, y_2)$. We will omit most technical details and mathematical subtleties here. Let us sample the solution of this ode at equal time-intervals $\{t_i = t_0 + i\Delta t\}$, and let us call these 'stroboscopic' values of the solution $\{s_i = y(t_i)\}$. The solution is uniquely

4 NONLINEAR STELLAR PULSATION

defined for all times provided we know its values at *two* anterior times. Thus any s_{i+1} can be predicted from the knowledge of two preceding values, say, s_i and $s_{i-\Delta}$, where Δ is an integer greater or equal to 1. Because we are dealing with a given differential equation there exists a function f such that $s_{i+1} = f(s_i, s_{i-\Delta})$, no matter what the time index i is. The form of this function depends of course on the differential equation and on the size of the time-intervals Δ .

It is convenient to introduce at this point the so called 'state vector'

$$\mathbf{X}_i = (s_i, s_{i-\Delta}) \quad (1.2)$$

and express the functional dependence with a map \mathbf{F} , viz.

$$\mathbf{X}_{i+1} = \mathbf{F}(\mathbf{X}_i). \quad (1.3)$$

The map \mathbf{F} moves us from a given state $\mathbf{X}_i = (s_i, s_{i-\Delta})$ to the next one $\mathbf{X}_{i+1} = (s_{i+1}, s_{i+1-\Delta})$ for all i . The state vector \mathbf{X}_i maps out a stroboscopic representation of the trajectory $y(t)$ in the two-dimensional 'phase-space' of the system. (This is a generalization of the usual physicist's definition of the phase-space corresponding to position and velocity or momentum, *c.f.* Weigend & Gershenfeld 1994). Because of the finite time-intervals the map \mathbf{F} is usually nonlinear, even if the differential equation were linear.

We have chosen a dynamics that is described by a second order differential system as an example only. In fact it is oversimplified for our purposes because irregular behavior can only occur for a flow in at least three dimensions and only in the presence of nonlinearity (Ott 1993). Generally then, when the signal of interest is generated by a higher dimensional dynamics, say a set of d coupled first order ode's, we merely need to increase the length or dimension of the vector to d

$$\mathbf{X}_i = (s_i, s_{i-1}, s_{i-2}, \dots, s_{i-d+1}) \quad (1.4)$$

and the map \mathbf{F} then operates in a d -dimensional phase-space, while \mathbf{X}_i describes the trajectory.

When confronted with an observational time-series we have no *a priori* knowledge, neither of the dimension d , nor of the form of the map \mathbf{F} . We shall call *embedding space* the space in which we try to reconstruct the dynamics. Suppose the embedding dimension d_e

that we have guessed is actually smaller than d , then clearly we cannot suitably describe the dynamical system. In particular the embedded trajectory will exhibit intersections which violates the uniqueness theorem of ode's. On the other hand there is nothing to be gained from making d_e greater than necessary. (This is very much akin to wanting to embed a 3-dimensional sphere in a plane which obviously is not possible. But, a 3D sphere remains a 3D sphere even when we embed it unnecessarily in 4 or 5 dimensions.) There exists thus a optimal, minimal embedding dimension $d_e^{min} = d$ (There are mathematical subtleties which sometimes can require $d_e^{min} > d$, but $d_e^{min} < 2d + 1$ c.f. *e.g.* Sauer *et al.* 1991.). One of our goals is to determine this d_e^{min} which then also gives an upper limit of the physical dimension d of the unknown dynamics. We shall also see below that another dimension, the fractal dimension d_L , sets a lower limit to d .

$$d_L \leq d \leq d_e^{min} \quad (1.5)$$

The two limits may coincide, as we have found in several examples, and in such lucky situations, the procedure uniquely determines the dimension d of the physical phase-space.

For the nonlinear map \mathbf{F} we make the simplest possible choice (for which there are also good mathematical reasons), namely we assume that \mathbf{F} is a sum of all the multivariate monomials up to some order p that we can form with the components of \mathbf{X}_i .

$$\mathbf{F} = \sum_k \beta_{\mathbf{k}} \mathcal{M}_{\mathbf{k}}(\mathbf{X}_i) \quad (1.6)$$

The $C_{p+d_e}^p$ vector coefficients $\beta_{\mathbf{k}}$ of these monomials can most easily be obtained by a linear least squares approach with the help of the singular value decomposition method (Serre, Kollath & Buchler 1996a, hereafter SKB96). Since the number of fitting coefficients increases very rapidly with p it is desirable to keep the latter as low as possible.

The flow reconstruction proceeds then as follows. We successively assume that the embedding dimension is $d_e = 3, 4, \dots$ and for each we determine the function \mathbf{F} , *i.e.* $\beta_{\mathbf{k}}$, by minimizing the error

$$\mathcal{E} = \sum_i ||\mathbf{X}_{i+1} - F(\mathbf{X}_i)|| \quad (1.7)$$

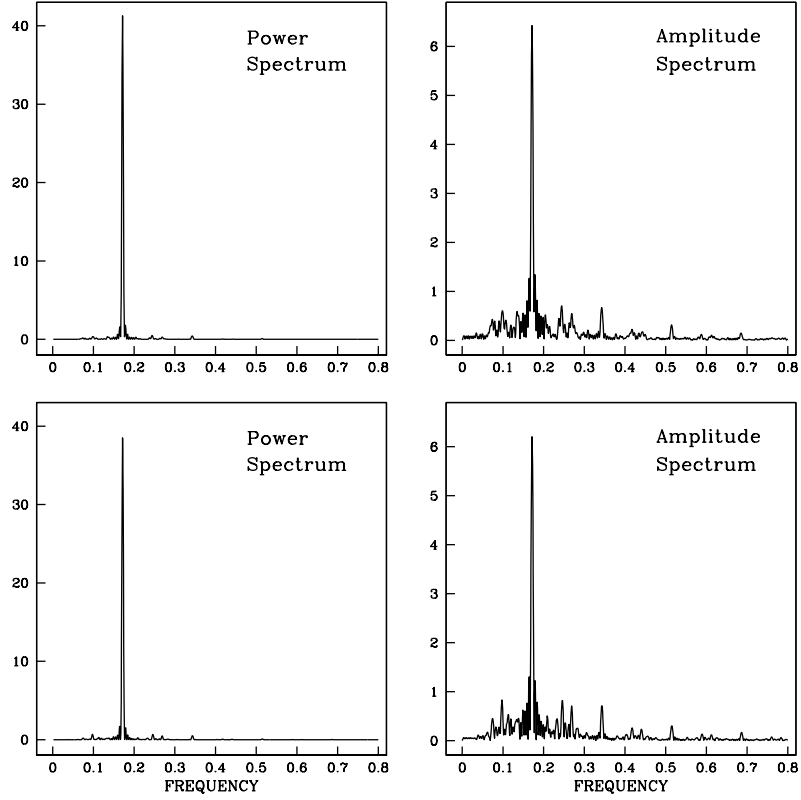


Figure 1.2 Fourier spectrum: Top: time-series ($t=0, 200$) of Fig. 1.1; Left: power, Right: amplitude; Bottom: Later segment of the same time-series ($t=1848, 2048$).

where $\|$ denotes the Euclidian norm, *i.e.* the square root of the squares of the components. For ideal noise-free data the error levels off sharply at a very small value (machine accuracy) when the minimum dimension d_e^{min} is obtained. For noisy data the error levels off at some finite value and the levelling-off is more gradual.

3. THE RÖSSLER OSCILLATOR

Can we have confidence that in practice the global flow reconstruction approach can really capture the dynamics of a system from the knowledge of the time dependence of merely one of its

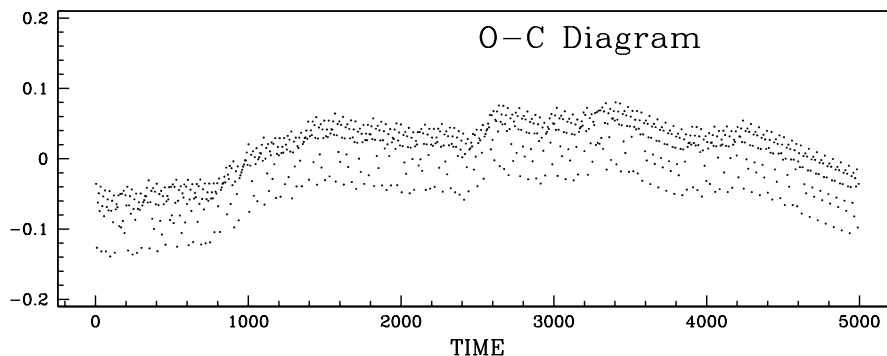


Figure 1.3 O-C Diagram of time-series of Fig. 1.1

variables? Can we also be sure that it does not erroneously find low dimensional chaos in any old irregular signal?

First we shall describe the behavior of the Rössler oscillator and then we present the results of a series of analyses that we have made on the time-series of the oscillator.

The Rössler system consists of an autonomous set of three first order ode's (Thompson & Stewart 1986).

$$\frac{dx_1}{dt} = -x_2 - x_3 \quad (1.8)$$

$$\frac{dx_2}{dt} = x_1 + ax_2 \quad (1.9)$$

$$\frac{dx_3}{dt} = b + (x_1 - c)x_3 \quad (1.10)$$

We have chosen the values $a = 0.2$, $b = 0.2$ and $c = 4.8$ for the tests.

This is a deterministic system of equations, yet for these parameter values, the solution of this system is irregular, *i.e.* remains bounded, but never repeats itself, and is very sensitive to initial conditions. This means that if we compute two solutions whose initial conditions differ by a tiny amount there will always arrive a time when the two solutions diverge, *e.g.* by oscillating out of phase, no matter how small the initial difference. In the domain of flows (which are differential systems as opposed to maps which are

discrete) the Rössler equations are the simplest known paradigm for what is called chaotic behavior.

In Fig. 1.1 displays a typical section of the temporal behavior of the variable $x_1(t)$ that we obtain from integrating the Rössler equations. One sees that there are wide fluctuations in amplitude. Yet, one notices that the phase is remarkably constant. It is therefore no surprise that the Fourier spectrum in Fig. 1.2 shows that the power is overwhelmingly in one frequency $f_0 = 0.17$, plus a little power in the first few harmonics. The more sensitive amplitude spectrum on the right shows some (unsteady) power in a broad region centered on $f_0/2$ and $3f_0/2$. It is unsteady in the sense that different sections of a long time-series would produce different structures.

Variable star observers have a predilection for O-C (observed minus calculated) diagrams which are plots of the time of appearance of a feature (say the light-curve maximum) relative to the corresponding multiples of the period. The intended purpose of these plots is to uncover evolution which, when linear in time, would show up as parabolic behavior. Because of its familiarity to observers we show such an O-C diagram for a long time integration of $x_1(t)$. It is clear that for an irregular signal such as the one we are discussing this diagram adds nothing to one's understanding of the nature of the small but real fluctuations in period. We recall that this system is *not* evolving, since the a , b and c parameters are constant!. One notes a banded pattern of clustering, for example, the higher concentration of points towards the top. Its origin will become clearer when we see that there is a quasi one-dimensional first return map that the dynamics follows ?, similar to the well-know logistic map (Ott 1993).

It turns out that the familiar linear analysis is not very useful either. To illustrate this we have made a Fourier fit to the time-series $x_1(t)$ of Fig. 1.1 (over 4000 time-units) with the twenty highest frequency peaks from the spectrum of Fig. 1.2. The resultant fit is shown as a solid line in Fig. 1.4 (left) together with $x_1(t)$ as a dashed line. The multi-frequency Fourier fit is excellent, which is not astonishing since one can obtain an arbitrarily good fit for a finite stretch of any time-series as one increases the number of frequencies in the fit. However, have we learned anything from such a fit about the time-series and how it was generated? If we have then this fit should have 'predictive' power, *i.e.* we should

be able to extrapolate it beyond the 4000 time-units and it should continue to give a good fit.

On the right side of Fig. 1.4 we show a continuation of the Fourier fit for the interval 20000 – 24000 time-units, superposed on the actual solution $x_1(t)$. The extrapolation deteriorates very quickly and at this stage is already very different from the signal. This shows that while it is possible to obtain a very good interpolation of a complicated time-series with a Fourier fit, the extrapolated signal bears little resemblance with the physical signal. Note that an ARMA process, which is also intrinsically linear, does not fare any better (SKB96). The obvious reason is that neither the Fourier fit nor the ARMA process capture the nonlinear behavior of the dynamics, and a more sophisticated technique is required.

In the observational astronomical literature one finds references to *nonlinearity* by which it is merely meant that the Fourier fit contains linear combination frequencies of some more basic frequencies. This could merely be indicative of mode-coupling in a multi-periodic signal. This 'nonlinearity' has little to do with the intrinsically nonlinear nature of a chaotic time-series that we are interested in here.

In contrast to the Fourier spectrum Fig. 1.5 gives very important information about the nature of the oscillations. These diagrams are what is known as 'first-return maps'. They are simply a plots of M_{k+1} versus M_k , where the $\{M_k\}$ are the successive maxima of the time-series (They could also be the minima, or any other characteristic point of the signal). On the left side we show the first-return map for the $x_1(t)$ variable of the Rössler oscillator. The right hand side displays the fits. The thick dots are the first return map of the multi-period Fourier fit, shown in Fig. 1.3 and the crosses the extrapolated fit.

The Rössler signal has a strong phase-coherence, and the first-return map has a very typical quadratic shape that is typical of very low dimensional chaotic systems (Ott 1993).

When we make a first-return map of the extrapolated Fourier fit we see that extrapolated signal gives a scatter plot whose scatter increases with the extrapolation time, showing again that while a multi-frequency Fourier fit gives a decent interpolation, it does not capture any of the physics that is in encrypted in the signal.

In SKB96 it is shown that the global flow reconstruction works very well. From $x_1(t)$ one can construct maps M that capture the

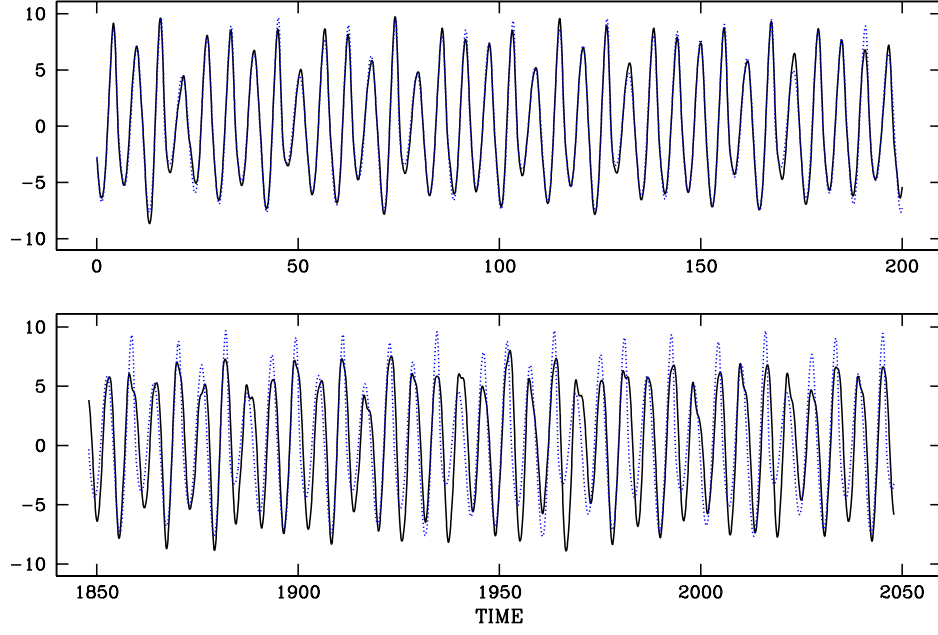


Figure 1.4 Fig. 1.5: Left: Fourier fit to time-series of Fig. 1.1 ($t=0,200$) ; right: Extrapolation of Fourier fit to $t=1848, 2048$.

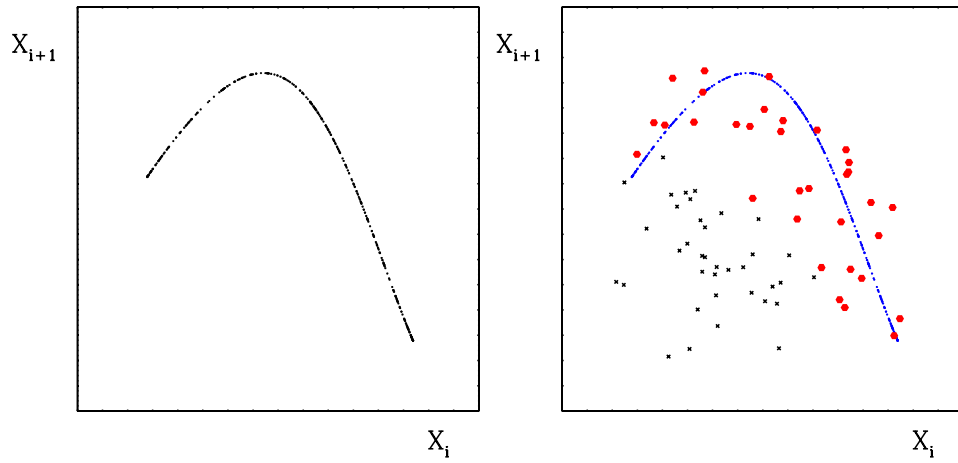


Figure 1.5 Left: First-return Map of the maxima of a long stretch of the original Rössler time-series; right; first-return maps for the interpolated (thick dots) and extrapolated (crosses) Fourier fit series, superposed on the original return map.

underlying Rössler dynamics. The success of the reconstruction manifests itself in several ways. From the maps we can generate 'synthetic' signals through iteration from a seed value. These synthetic signals have the same appearance as the training set $x_1(t)$ that was used to generate the maps. The maps and synthetic signals are robust, *i.e.* they are independent of some of the arbitrary parameters such as the delay Δ or the maximum polynomial order p over a comfortable range of values. Of course in the comparison it must be kept in mind that in view of the chaotic nature of the signal it does not make any sense to compare two time-series point by point. Only average, global properties, matter.

In order to see whether the method might still, and perhaps erroneously, predict low dimensional chaos SKB96 made the following test of the flow reconstruction method using a stochastic signal with superficially very similar properties as the Rössler time-series. A test signal was constructed by prewhitening $x_1(t)$ with the frequency 0.171 that dominates the Fourier spectrum, as well as its first eight harmonics. The remaining signal (which is quite erratic) is then Fourier analyzed, and we compute the envelope of the complex amplitude spectrum and convolve its inverse Fourier transform with a white noise signal. The colored noise that we have thus generated is then added to the original periodic pre-whitening signal to give our test signal. The appearance of the signal is essentially the same as $x_1(t)$ and its Fourier spectrum, by construction, is also very similar.

The important result of this test is that the flow reconstruction method was not fooled into believing that this stochastic test time-series is a low dimensional signal (SKB96).

Dynamicists have developed other characterizations of chaotic time-series and of the underlying chaotic attractor. Of particular interest to us are the Lyapunov exponents which measure the degree of convergence or divergence of neighboring trajectories (Ott 1993). Unfortunately, observational data sets of irregular or Semi-Regular variable stars are generally much too short to allow us to compute Lyapunov exponents or a fractal dimension with any reliability. However, once we have constructed the map or flow, we can use the latter to compute the Lyapunov exponents, and from these the

fractal dimension

$$d_L = K + \frac{1}{|\lambda_{K+1}|} \sum_{i=1}^K \lambda_i \quad (1.11)$$

where the λ_i are the Lyapunov exponents, ordered decreasingly, and K is the largest value such that the sum is positive.

If, as a test, we only take a short time-series of the Rössler oscillator we could show that the Lyapunov dimension d_L is reproduced quite accurately via our flow reconstruction procedure, *e.g.* one finds $d_L \approx 2.014$ instead of the exact value of 2.013 (SKB96).

It might appear that we are getting a free lunch with this roundabout way of computing the Lyapunov dimension via the synthetic time-series. This is not so. We have indeed used additional information, namely we have made the working assumption that the signal is generated by a deterministic low dimensional dynamics. As an illustration of this point suppose for example that we know that we are given a temporal data set that has been generated by a second order differential equation. From this we know that we can fit the time-series with a map or flow that related only two successive points, and we can recover the original differential equation and the general properties of its solution.

We have not yet talked much about the delay Δ . If we choose Δt too small, the \mathbf{X}_i are very similar and the map \mathbf{F} becomes close to linear. However, then the construction of \mathbf{F} is dominated by the noise. On the other hand, when Δ is too large, the function \mathbf{F} becomes very nonlinear and we are obliged to go to high order monomials (large p) with a concomitantly large number of coefficients to be determined. Clearly we have to choose an intermediate regime, and the confidence in our reconstruction is enhanced when this regime is sufficiently broad.

We note that in all the dynamics that we have reconstructed, namely the test case of the Rössler oscillator (SKB96), the pulsations of a hydrodynamic Pop. II Cepheid (W Vir) model (Serre *et al.* 1996b), the observed light-curves of R Scuti (Buchler, Serre Kolláth & Mattei 1995 [BSKM95]; Buchler, Kolláth, Serre & Mattei [BKSM96]) and of AC Herculis (Kolláth, Buchler, Serre & Mattei 1998) we have found that indeed the results are stable over a range of Δ values.

So far we have discussed only the search for a *map* that describes the temporal evolution of the system in a stroboscopic sense. It

is also possible to determine directly the differential system (flow) (Eq. 1.1) that describes the system system. A direct determination of the flow is slightly more delicate (SKB96).

4. VARIABLE STARS

Variable stars are of course more complicated than the simple paradigm of the 3D Rössler system. First, we are dealing with an infinite dimensional system since a star has an infinity of modes of oscillation. However, the relative simplicity of dissipative systems as opposed to Hamiltonian ones, is that the evolution does not occur the full infinite-dimensional phase-space, but only in a subspace of finite, and often small, dimension. Examples best known to the reader are the mono-periodic pulsations of ordinary Pop I Cepheids and RR Lyrae that occur in a mere 2D phase-space (in which the variable is the complex amplitude of the excited mode), or the beat Cepheids, double-mode RR Lyrae and bump Cepheids that occur in a 4D phase-space because here two pulsation modes are involved. One hopes, and one indeed finds, that the same 'dimensional reduction' remains true for the more complicated, and highly irregular pulsations of W Vir and RV Tau stars.

There is another difference at a more subtle level. In the previous section, when we studied the dynamics of the Rössler oscillator we used one of the phase-space variables, namely $x_1(t)$, in the reconstruction. In the stellar case we have at our disposal only the temporal behavior of the luminosity which is not a phase-space variable. It can be shown however (*e.g.* Abarbanel *et al.* 1993, Weigend & Gershenfeld 1993) that even so we can infer the properties of the dynamics provided that the luminosity contains all the information about the dynamics, in other words provided that L is a generic function of the phase-space variables. The strong coupling between the heat flux and the pulsation variables (radii and velocities) guarantees that the luminosity is indeed a 'good' variable.

When dealing with observational data two further practical complications arise. First, observations are never made at equally spaced time-intervals and we need to interpolate, which introduces errors or noise. Second, there is also observational noise, and if the noise level is too high it may be very difficult or impossible to extract the dynamics from the time-series.

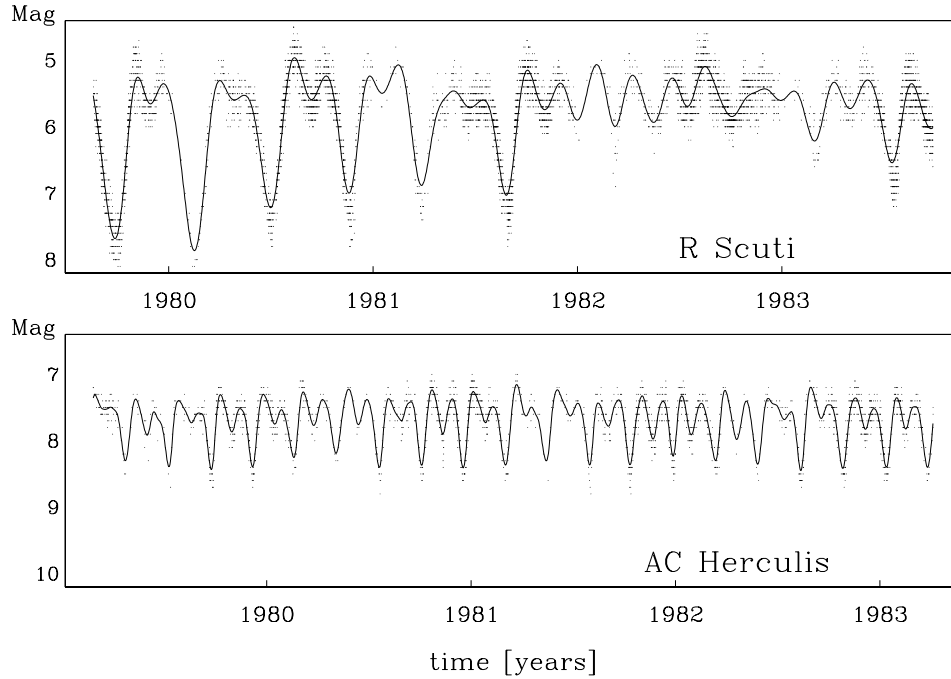


Figure 1.6 Segments of the AAVSO light-curve data and our spline-fits.

Very few observational data sets in which one may expect low dimensional chaos are sufficiently long and sufficiently densely sampled to perform a flow reconstruction. Fortunately the AAVSO has archived amateur astronomer observations of variable stars over the years. There are two such stars, R Scuti and AC Herculis, belonging to the RV Tau type of Pop II Cepheids that undergo irregular pulsations of large amplitude and are very bright, and thus have been observed very assiduously by amateur astronomers. Because the observations are mainly visual, the observational errors are relatively large, ~ 0.1 mag, but because there are a lot of statistically independent data we can still extract a reasonably accurate light-curve.

In Fig. 1.6 we display small sections of the observational data of R Sct and AC Her superposed on our spline-fit that we use for the reconstruction. The observational error is the same for the two stars, but the amplitude is smaller for AC Her so that the latter has a worse signal-to-noise ratio than AC Her.

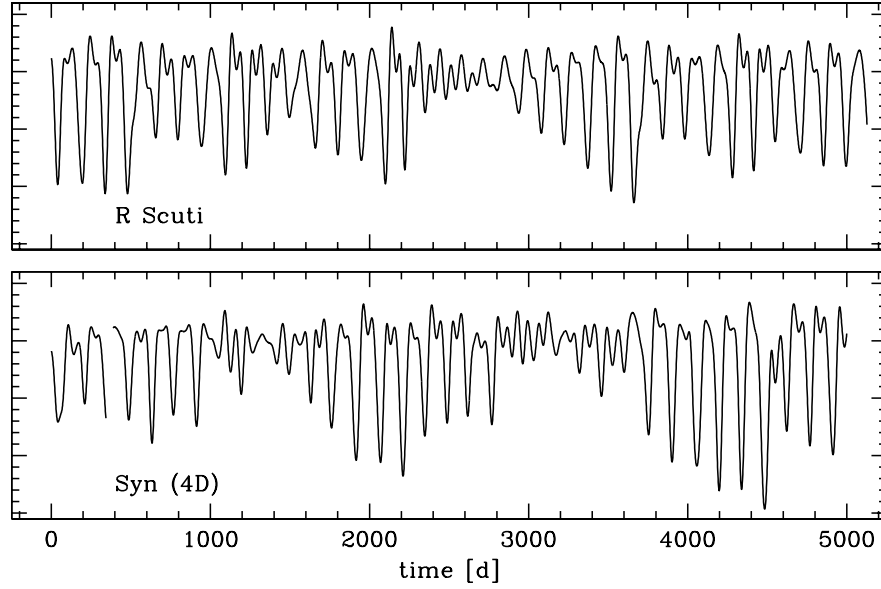


Figure 1.7 Top: R Sct light-curve; Bottom: synthetic fit (see text)

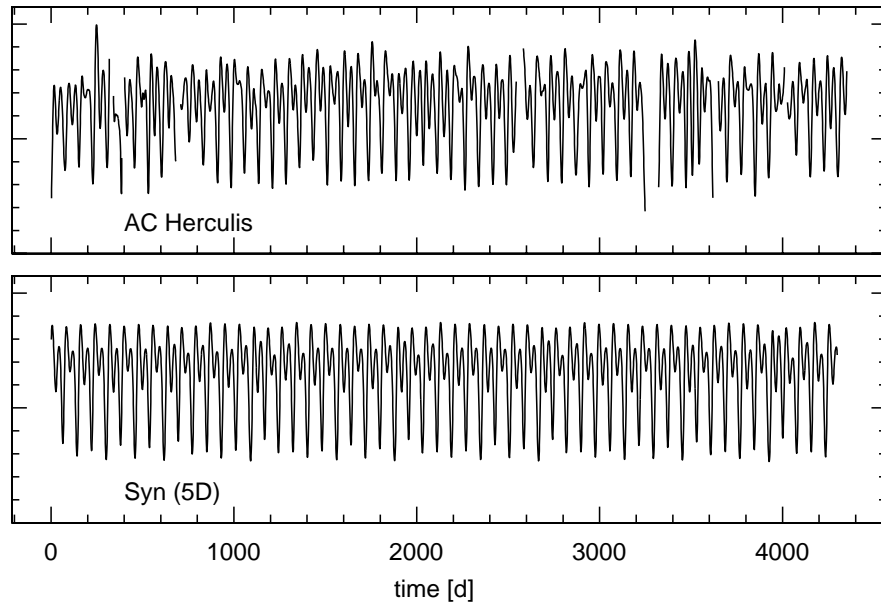


Figure 1.8 Top: AC Her light-curve; Bottom: synthetic fit (see text)

The complete time-series that we have utilized for our flow reconstruction are shown in the top sections of Fig. 1.7 for R Sct, and in Fig. 1.8 for AC Her. The corresponding amplitude Fourier spectra are displayed in Fig. 1.9.

R Scuti

In a Fourier analysis of 150 years of R Sct light-curve data it was shown by Kolláth (1990) that the Fourier spectrum has a more or less constant envelope with large peaks in the broad vicinities of $\approx 0.07d^{-1}$ and its harmonic. But the spectrum is not steady since for successive segments of the data the individual peaks occur in different places and without any smooth transition between them. This rules out the light-curve as being that of an evolving multi-periodic star. Consequently, while multi-periodic fits might provide good interpolations of the light-curve, they are useless from a physical point of view because they add no new understanding of the mechanism for the irregular behavior.

In BSKM95 and BSKM96 it was further demonstrated that an ARMA process cannot underlie the light-curve. Again, it is not astonishing that such a linear analysis does not work either because they are not independent. Fortunately, an ARMA process does not capture the dynamics, because if it did one would be hard pressed to come up with a stochastic mechanism that can give rise to factors of 40 fluctuations in luminosity!

There is no point in repeating the detailed analysis of R Sct that has been described in BSKM96. That paper followed the procedure outlined in §3. Starting with dimension $d_e > 2$, maps were constructed in spaces of increasing dimension and for a range of values of time-delay Δ and maximum polynomial order p . Once one has obtained such maps, one can easily iterate them starting with a seed value and thus generate synthetic signals. One of the criteria for claiming success is that such synthetic signals have the same properties, in particular the same appearance, as the stellar data that were used to generate the maps. The resemblance of these synthetic signals with the observational data is an indication that our reconstructed map has captured the dynamics, but additional tests have to be made to validate the reconstruction.

For R Sct all attempts to obtain faithful maps failed in 3D. But BSKM96 found that it was possible to obtain maps that show ro-

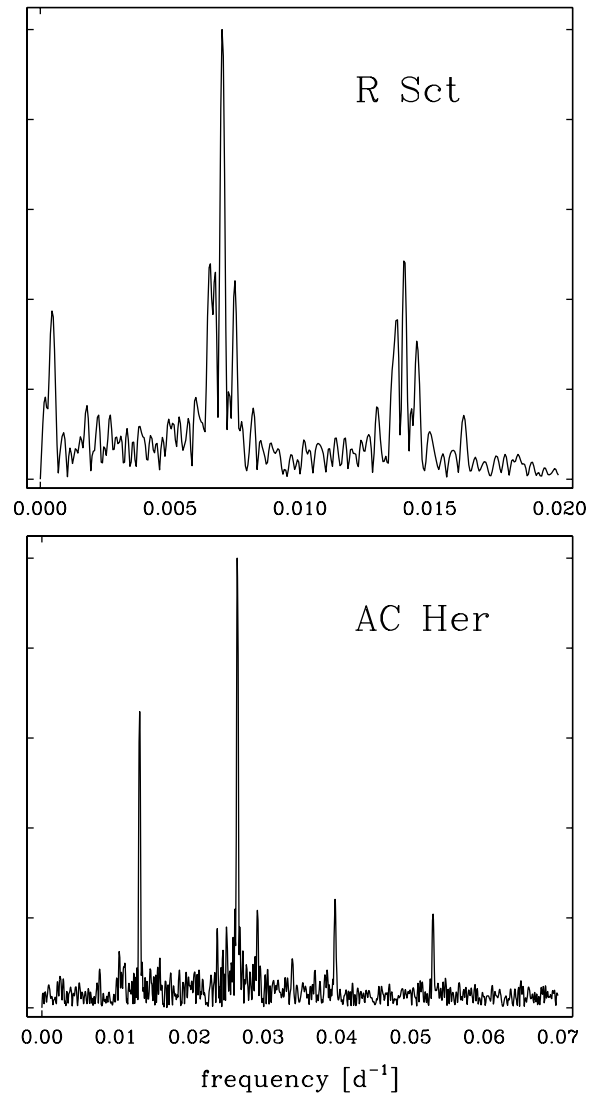


Figure 1.9 Amplitude Fourier spectra of R Sct and AC Her.

bustness within some range of delays Δ and polynomial nonlinearity p for embedding dimensions greater of equal to four. The minimum embedding dimension for R Sct is therefore $d_e^{min} = 4$.

Because of the shortness of the observational time-series it is not possible to derive Lyapunov exponents directly from the data, but these exponents can be derived from the maps or from the synthetic signals. BKSM96 found that the Lyapunov exponents also show good robustness, and that they indicate a fractal dimension of $d_L \approx 3.1$. What is important is that this dimension is essentially invariant even when the embedding dimension d_e is as large as 6.

The fractal dimension of the attractor imposes a lower bound of $d_L \leq d$ on the dimension of phase-space, whereas the minimum embedding dimension $d_e \leq d$ imposes an upper bound of 4. In the case of R Sct the upper and lower bounds agree and we can conclude that the dimension of the physical phase-space is $d = 4$.

What is the physical meaning of this dimension? This becomes clear when we look at the linear eigenvalues of the map about the fixed-point, which correspond to the linear vibrational stability of the star. We have displayed these quantities for our best map in Table 1.1. The stability roots are written in the form $\exp(\rho + i\nu)$. Negative and positive ρ therefore denote linear stability and instability, respectively. The (angular) frequency eigenvalue, $\nu_1 = 0.0068$ is close to the average cycling frequency of the light-curve, whereas the higher frequency is almost double its value. The lower frequency is unstable and the higher frequency is stable. Because we can associate these eigenvalues with vibrational modes this then leads to the nice and simple physical picture: The 4D phase-space that we have uncovered in the light-curve of R Sct is spanned by two vibrational modes, a linearly unstable mode and a resonant, linearly stable overtone. One can therefore interpret the irregular pulsation as a continual exchange of energy between two pulsation modes, one that wants to grow and one, with approximately twice the frequency, that wants to decay.

Why do Pop II Cepheids such as R Sct behave so differently from their Pop I siblings? The reason is that they have much larger relative growth-rates $\eta = 2\kappa P$. In the classical, Pop I Cepheids the growth-rates of the excited modes are generally of the order of a percent or less. This means that amplitude variations can only occur on time-scales of hundreds of pulsations, whereas the

relative growth-rates of the Pop II Cepheids are of the order of 0.5 or greater. Obviously irregular behavior can only occur when the amplitude can change on a time-scale of a period. The reason that Pop II Cepheids have higher relative growth-rates is due to their higher luminosity/mass ratio – the coupling between the radiative flux and the pulsation is therefore much stronger. In the jargon of stellar pulsation theory, these stars are much more nonadiabatic.

Table 1.1 Linear stability roots of fixed point of the R Scuti maps

ν_1	ρ_1	ν_2	ρ_2
0.0068	0.0044	0.0145	-0.0062

One final comment. One might object that it may be possible to generate a map, but that there does not necessarily exist any flow of which the map is the stroboscopic manifestation. In our analysis of R Scuti we have used delays Δ corresponding to a day (compared to the cycling time of 70 days). Because of these fine time-steps the map \mathbf{F} is very close to a (differential) flow. We find that one of the Lyapunov exponents is always close to zero (For a flow it should be rigorously zero.) This further corroborates our belief that we have captured the dynamics of the star.

AC Herculis

The analysis is more delicate for the AC Her data which, as we have already pointed out, have a smaller sign-to-noise ratio. Details of the reconstruction are described in Kolláth, Buchler, Serre & Mattei (1998). The best map one can obtain is not as satisfactory as for R Sct. A synthetic light-curve is shown in the bottom of Fig. 1.8. The fractal dimension turns out to be a little smaller, $d_L \approx 2.3$, presumably because of the more regular behavior of the light-curve compared to R Sct.

Before finishing this section we want to point out that the same flow reconstruction method has also been applied to the solar cycle problem by Serre and Nesme-Ribes (1997, 2000).

Data requirements

An observer may want to know what the best strategy might be for observing an irregular variable star. This is a difficult question to answer in a general sense, but some general comments are possible (*c.f.* SKB96). We recall that we want to be able to construct as many as possible \mathbf{X}_i vectors with the least amount of noise, therefore

(a) the signal-to-noise ratio has to be large enough so that the stochastic behavior does not overwhelm the deterministic one;

(b) it is important to have very good coverage – this may be 20 or more points per cycle. If we have to interpolate over small gaps this is equivalent to introducing noise which destroys our ability to extract the dynamics; larger gaps are ok as long as the star (and its dynamics) does not change during the gap.

(c) the time-series must be typical of the dynamics. By that we mean that it must explore essentially all of phase-space. Common sense tells us that if, for example, the signal has long term modulations, then it is necessary to take a stretch of data that is long enough to sample those modulations.

5. TIME-FREQUENCY ANALYSIS

In this section we discuss the application of modern time-frequency analysis to variable star data, even though it is a *strictly linear analysis*. The reason is that one can gain a useful overview of how the signal changes in time, and, as we see, it confirms our conjecture about R Scuti’s pulsations as being due to the continual exchange between two modes of pulsation. We stress though that this approach, as all other linear ones, is purely interpolative, has little if no extrapolative potential, and therefore does not allow us to gain information about the nonlinear physical nature of the source of the signal.

The Transforms

The Fourier transformation of $s(t)$

$$S(\omega) = \mathcal{F}_{t,\omega}[s(t)] = \int s(t) \exp(-i\omega t) dt$$

is widely used to determine the spectral content of stationary signals. However for time-series with variable frequency content the

Fourier spectrum can tell nothing about the temporal variation. Note that we use the above notation for the Fourier transformation herein, and $\mathcal{F}_{t,\omega}^{-1}[S(\omega)] = 1/(2\pi) \int S(\omega) \exp(i\omega t) d\omega$ for the inverse Fourier transformation.

A variety of techniques that are extensions of Fourier analysis to nonsteady time-series, such as Gábor transforms and wavelet analysis, and more sophisticated time-frequency distributions, have made it into the astronomical literature over the last decade. A nice general reference to time-frequency analysis is Cohen (1994). Several applications to astronomical data have been summarized in recent workshop proceedings (*e.g.* Buchler & Kandrup 1997).

The spectrogram *i.e.* the square of the short time Fourier transform (STFT) is a classical tool of time Frequency analysis. The general form of STFT is given by:

$$G(t, \omega) = \mathcal{F}_{\tau, \omega} [s(\tau) h^*(\tau - t)], \quad (1.12)$$

where the kernel $h(t)$ performs a local (in time) weighting on the signal. The STFT introduced by Gábor (1946), who used a Gaussian kernel:

$$h(t) = \exp(-t^2/(2\sigma^2)). \quad (1.13)$$

We refer to this special STFT as the Gábor transform.

Wavelets are also frequently applied for astronomical data sets, although they do not perform as well as the other methods. Here we note only that replacing the constant σ in the Gábor kernel (Eq. 1.12) by $\sigma(\omega) = \omega/c$ results in the Morlet wavelet. With this connection a numerical realization of the Gábor transform can be easily changed to wavelet and vice verse.

The simplest member of a more general class of time-frequency distributions (see Cohen 1966) is the Wigner distribution (WD) (Wigner 1932):

$$W(t, \omega) = \int \exp(-i\tau\omega) s^*(t - \frac{\tau}{2}) s(t + \frac{\tau}{2}) d\tau \quad (1.14)$$

$$= \mathcal{F}_{\tau, \omega} \left[s^*(t - \frac{\tau}{2}) s(t + \frac{\tau}{2}) \right] \quad (1.15)$$

The WD has numerous advantages, like the properties of marginals, it recovers the nature of a chirp signal exactly etc. However, because of the nonlinearity of the transformation, the WD of multicomponent signals is contaminated by cross terms (see Cohen 1989).

The advantageous properties of the WD can be further expanded with more flexibility in the Cohen's class of TFD's (Cohen 1966):

$$C(t, \omega) = \frac{1}{2\pi} \int \int \int \exp(-i\xi t - i\tau\omega + i\xi\theta) \Phi(\xi, \tau) s^*(\theta - \frac{\tau}{2}) s(\theta + \frac{\tau}{2}) d\theta d\tau d\xi, \quad (1.16)$$

where $\Phi(\xi, \tau)$ is the kernel of the distribution. The Wigner Distribution is a special case by the unit kernel ($\Phi(\xi, \tau) = 1$).

Alternatively C can be expressed in the terms of the WD according to:

$$C(t, \omega) = \frac{1}{2\pi} \int \int \varphi(t - \theta, \omega - \xi) W(\theta, \xi) d\theta d\xi. \quad (1.17)$$

Here φ is the 2D Fourier transform of the kernel Φ :

$$\varphi(t, \omega) = \mathcal{F}_{t, \xi}^{-1} [\mathcal{F}_{\tau, \omega} [\Phi(\xi, \tau)]] . \quad (1.18)$$

If φ is a low-pass filter in the time-frequency plane, then the TFD is a smoothed version of the WD. The smoothing compresses the cross terms, but decreases the resolution in the distribution.

For the numerical realization it helps to calculate the TFD's through Fourier transformations. It is easy to see that Eq. 1.16 can be written in the following form:

$$C(t, \omega) = \mathcal{F}_{\tau, \omega} \left[\int \hat{\varphi}(t - \theta, \tau) s^*(\theta - \frac{\tau}{2}) s(\theta + \frac{\tau}{2}) d\theta \right], \quad (1.19)$$

where $\hat{\varphi}(t, \tau) = \mathcal{F}_{t, \omega} [\Phi(\omega, \tau)]$. The TFD is the Fourier transform of the local autocorrelation

$$R_t(\tau) = \int \hat{\varphi}(t - \theta, \tau) s^*(\theta - \frac{\tau}{2}) s(\theta + \frac{\tau}{2}) d\theta \quad (1.20)$$

For our applications we use the TDF kernel defined by Choi and Williams (1989): $\Phi(\xi, \tau) = \exp(-\theta^2 \tau^2 / \sigma)$, giving the following distribution. Then in Eq. 1.19 the weighting function for the local autocorrelation becomes:

$$\hat{\varphi}(t, \tau) = \frac{1}{2\pi^{1/2}} \left(\frac{\sigma}{\tau^2} \right)^{1/2} \exp \left(-\frac{t^2}{4} \frac{\sigma}{\tau^2} \right). \quad (1.21)$$

We note that the separable exponential kernel:

$$\Phi(\xi, \tau) = \exp(-\tau^2 / \alpha^2 - \beta^2 \xi^2) \quad (1.22)$$

is also very effective in suppressing the cross terms, but contrary to the Choi-Williams distribution a TFD with this kernel does not satisfy the marginals. The separable exponential kernel has a special property, *e.g.* with $\alpha = \beta$ it reproduces the Gábor transform, while with $\beta \ll \alpha$ the distribution converges to the WD. This makes it possible to get a continuous set of TFD's connecting the Wigner distribution to the STFT.

One cannot claim *a priori* that any one of these methods is generally superior to the others. This depends largely on the nature of the signal and of what features one tries to enhance, and it is therefore advantageous to use simultaneously several of them.

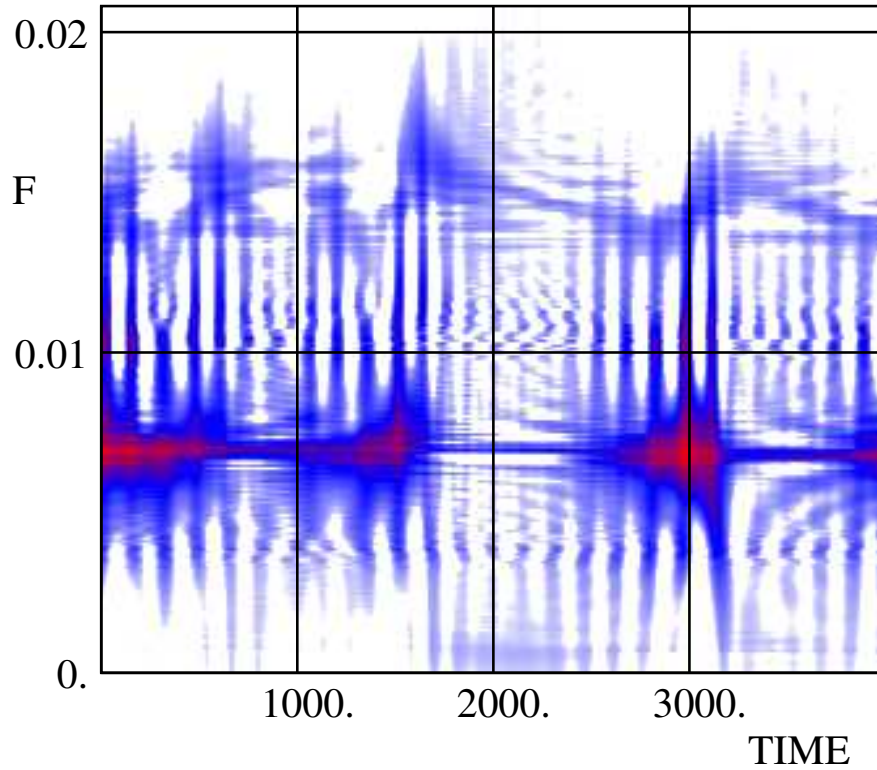


Figure 1.10 Choi Williams distribution of the synthetic R Sct light-curve

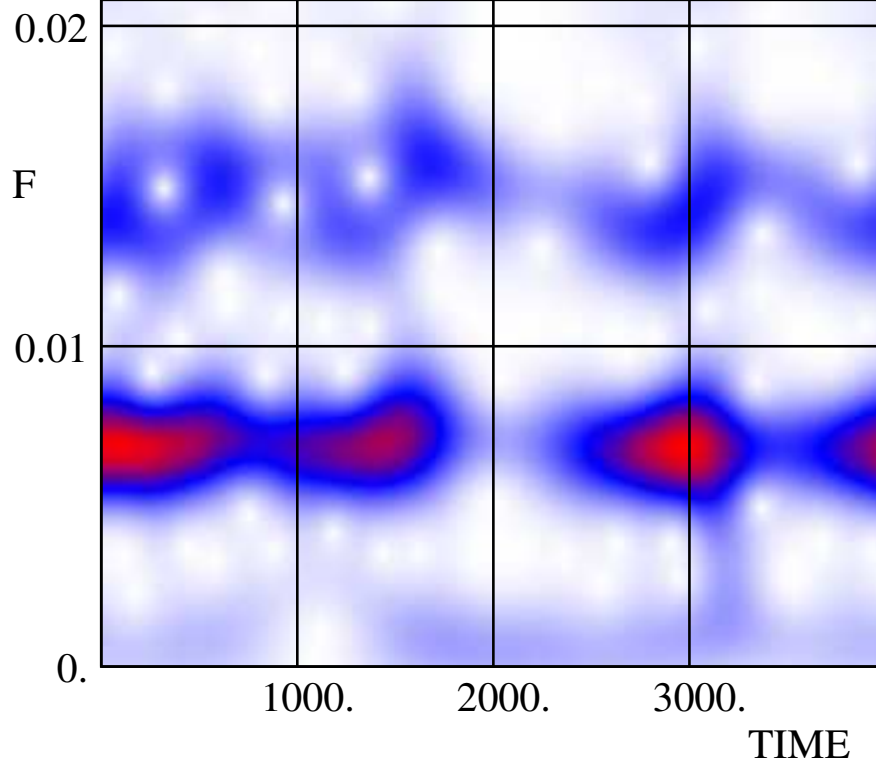


Figure 1.11 Gábor transform of the synthetic R Sct light-curve

Application

We demonstrate the power of time frequency distributions on a synthetic signal obtained by the iteration of the map fitted to the R Sct observations (BKSM96). We selected a 4000 day long data segment (top curve in Fig. 1.13) of a synthetic R Sct light-curve for the time frequency analysis. As we have already shown in Table 1.1 the linear stability analysis of the fixed point of this map uncovers a pair of frequencies $f_o \approx 0.007$ c/d and $f_1 \approx 0.016$ c/d. The interaction of these two spiraling manifolds is very important in the dynamics of the map. The above mentioned frequencies and $2f_o$ manifest themselves in the Fourier spectrum but with broad structures of peaks.

Fig 1.10 shows the Choi-Williams distribution of the synthetic data. The amplitude modulation of the different frequency compo-

nents and the shift between the frequencies $2f_o$ and f_1 are clearly visible in the time-frequency representation of the signal. This effect is the result of the interaction of the two spiral manifolds.

For comparison we have also shown the Gábor transform for the same signal in Fig. 1.11. Although the same overall features are the same in the Gábor transform the latter appears like an out-of-focus version of the much sharper Choi-Wiliams distribution.

In the study of multi-component signals with strong modulations it is usually fruitful to decompose the signal for its physically relevant components. The analytic signal formalism (see Kolláth and Buchler in this Volume) can be used to obtain the instantaneous amplitudes and periods of the different components. In Figure 1.12 we present the real part of the filtered analytic signal for the three main components around the frequencies f_o , $2f_o$ and f_1 . The half width of the filtering was set to 0.0015 c/d. The amplitudes of f_o and its harmonic $2f_o$ are correlated as expected. The two higher frequency components cannot be exactly separated because of the small frequency difference, but the most important tendencies are visible. The amplitude of the f_1 component starts to increase at the maximum amplitude of the lower frequency part.

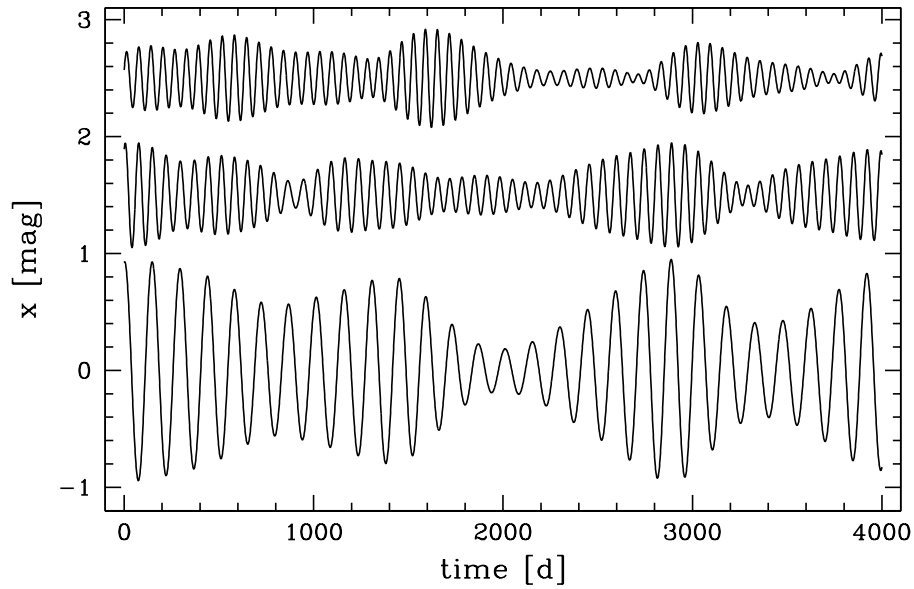


Figure 1.12 The decomposition of the signal presented in Fig. 1.13: lower curve: f_o , middle: $2f_o$, top: f_1 .

To check the quality of the decomposition, the sum of the components together with the original synthetic variation is presented on Figure 1.13. Although some of the local features are missed in the three component representation, it gives a nice agreement with the data. The amplitude is slightly decreased because of the windowing in Fourier filtering.

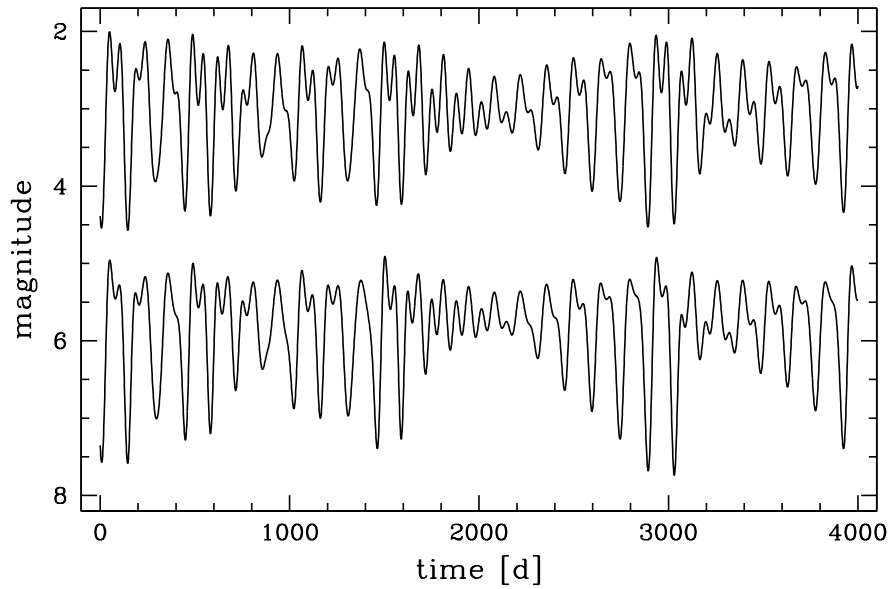


Figure 1.13 The synthetic light-curve from the R Sct map (top) and the sum of its three primary components (bottom).

For the R Sct light-curve itself the frequency separation of the higher frequency components appear somehow smaller, and it is difficult to accurately decompose those parts, but the various TFD's still can recover the variable frequency content around $f=0.015$ c/d. In an application to the light-curve of the star Kolláth & Buchler (1997) found that the standard wavelet analysis gave very little insight, but that the Gábor transform and the Choi-Williams distribution showed a systematic wavering of power in the neighborhood of twice the basic frequency. During the phase when the pulsation amplitude of the linearly unstable basic pulsational mode of frequency f_0 grows, the amplitude of its first harmonic ($2f_0$) grows concomitantly, but during the phase when the linearly stable, but resonant overtone mode with a frequency $\gtrsim 2f_0$ dominates (and the

verall amplitude decays) we see the frequency power shift from $2f_0$ to a frequency $\gtrsim 2f_0$. This picture supports the basic properties of the map that were obtained with the flow reconstruction method described in the previous section.

We end this section by stressing again that the time-frequency analysis, being linear, it cannot capture the nonlinearity of the dynamics.

6. TOPOLOGICAL ANALYSIS

The topological analysis is much more mathematical and its description is beyond the scope of this review. We therefore only give the gist of it here and we refer to Letellier & Gouesbet (1997) and Letellier *et al.* (1996) for a detailed description and its application to variable stars. The topological analysis can be very useful in characterizing and comparing different time-series and their underlying attractors, but it is limited to three-dimensional dynamical systems and in addition to those that have a large intrinsic dissipation.

Chaotic attractors can be regarded as the set of all their unstable orbits (Ott 1993). If these orbits are not too unstable, *i.e.* the system stays in such an unstable orbit for a good fraction of a period and if a sufficient number of visits occur in the span of the time-series then we are able to extract enough information about these orbits to characterize them. The way these orbits are braided in phase-space gives us a characteristic fingerprint of the attractor (and thence the dynamics). The method extracts information about the lowest few unstable orbits of the attractor, sets up a template for the attractor, and then checks that the higher unstable orbits appear in the order predicted by the template.

The restriction of the analysis to 3D comes from the fact that the analysis makes use of knot theory (for which there is no theory in 4D). On the other hand, the restriction to large dissipation is required if we are to be able to characterize the organization of the attractor into bands. This requires then that the fractal dimension of the attractor be $2+\epsilon$, with $\epsilon \lesssim 0.1$.

So far the method has been successfully tested on and tried on the Rössler oscillator and applied to the nonlinear pulsations of models of W Virginis stars. It turns out that the dynamics of the W Virginis model is very similar to the Rössler dynamics, although

the templates of the dynamics are slightly different (*c.f.* Letellier & Gouesbet 1996) and Letellier *et al.* 1997)

The fractal dimensions of the attractor of R Scuti (~ 3.1) and of AC Herculis (~ 2.3) are unfortunately too large for this method to work though. This lack of applicability can also be inferred from the shapes of the first-return maps of these pulsating stars (Buchler, Kolláth & Serre 1995, Figs. 4 and 5) which are certainly not 1D. The topological analysis relies on the existence of a fairly well defined first-return map in order to define a symbolic dynamics and the pruning tree (nature and order appearance of the higher order unstable orbits).

7. CONCLUSIONS

We have discussed how the standard linear techniques of time-series analysis become useless when the aim is to understand the nature of an intrinsically nonlinear time-series. We have presented two recently developed tools, the flow reconstruction method and the topological method, both of which take the nonlinear nature of the signal into account.

The irregular variability of the Semi-Regular variables had remained a mystery for a long time. With the help of the flow reconstruction approach it has now been solidly established that this irregular variability is the result of a chaotic dynamics that governs the behavior of these stars. The approach has also laid bare the physical mechanism: the irregular variability comes from the nonlinear and resonant interaction of just two radial pulsation modes, one linearly unstable and the other linearly stable, but with approximately twice the frequency of the first. It is the highly nonadiabatic nature of these modes that allows amplitude variations to occur on the time-scale of a 'period'. Future research will have to show how and why the pulsations of the Pop II Cepheids, comprising the W Virginis and RV Tauri type stars, become increasingly complicated as their luminosity increases. A good quantitative understanding of this behavior would generate a tool for nonlinear asteroseismology.

The topological analysis has been applied to the nonlinear pulsations of a model for a W Virginis type star, confirming the chaotic nature of the pulsations and giving a quantitative comparison with the Rössler system. The method will be very useful for the analysis

of the light-curves of W Virginis type stars when they become available. The pulsations of their more luminous siblings, the RV Tauri type stars are unfortunately too high dimensional for this method.

Finally, we have discussed a time-frequency method. This linear method is purely descriptive, but it is useful for shedding light on the nature of unsteady pulsations in that it shows the temporal variations of the modal content of the pulsations.

Acknowledgments

It is a pleasure to acknowledge valuable discussions with our collaborators Thierry Serre, Gerard Gouesbet, Christophe Letellier and Janet Mattei. This work has been supported by the National Science Foundation (AST95-28338, AST98-19608) and by the Hungarian OTKA (number T-026031).

References

- Abarbanel, H.D.I., Brown, R. Sidorowich, J.J., *et al.* (1993). The analysis of observed chaotic data in physical systems. *Rev. Modern Physics*, 65:1331-1392.
- Buchler, J. R., (1997). Search for Low-Dimensional Chaos in Observational Data. – in *International School of Physics "Enrico Fermi", Course CXXXIII, Past and Present Variability of the Solar-Terrestrial System: Measurement, Data Analysis and Theoretical Models*, Eds. G. Cini Castagnoli & A. Provenzale, Societ Italiana de Fisica, Bologna, Italy. pp. 275–288.
- Buchler J. R. and Kandrup, H. (1997). *Nonlinear Signal and Image Analysis*, *Ann. N.Y. Acad. Sci.*, Vol. 808.
- Buchler, J. R., Kolláth, Z. & Serre, S. (1995). Chaos in Observational Data of Variable Stars –Irregularity from the Nonlinear Interaction of Standing Waves? – in *Waves in Astrophysics*, Eds. J.H. Hunter, R.E. Wilson, *Ann. N.Y. Acad. Sci.*, 773:1–13.
- Buchler J. R., Kolláth, Z., Serre, T. and Mattei, J. (1996). A Nonlinear Analysis of the Variable Star R Scuti. *Astron. Astrophys.*, 311:833–844. [BKSM96]
- Buchler, J. R., Serre, T., Kolláth, Z. & Mattei, J. (1995). A Chaotic Pulsating Star – The Case of R Scuti *Physical Review Letters* 74:842–845. [BSKM95]
- Cini Castagnoli, G. & Provenzale, A. (1997). – in *International School of Physics "Enrico Fermi", Course CXXXIII, Past and Present Variabil-*

- ity of the Solar-Terrestrial System: Measurement, Data Analysis and Theoretical Models*, Eds. G. Cini Castagnoli & A. Provenzale, Societ Italiana de Fisica, Bologna, Italy.
- Choi, H.I. and Williams, W.J. (1989). Improved time-frequency representation of multicomponent signals using exponential kernels. *IEEE Trans. Acoust., Speech, Signal Proc.*, 37:862–871
- Cohen, L. (1966). Generalized phase-space distribution functions. *J. Math. Phys.*, 7:781–786
- Cohen, L. (1989). Time-frequency distributions – a review. *Proc. IEEE.*, 77:941–981
- Cohen, L. (1994). Time-Frequency Analysis. Prentice-Hall PTR. Englewood Cliffs, NJ
- Gabor, D. (1946). Theory of communications. *J. IEEE (London)*, 93:429–457.
- Kolláth Z. (1990). Chaotic Behaviour in the Light Variation of the RV Tauri Star R Scuti *M.N.R.A.S.*, 247:377–386.
- Kolláth, Z. and Buchler, J. R. (1996). Time-Frequency Analysis of Variable Star Light Curves. – in *Nonlinear Signal and Image Analysis*, *Ann. N.Y. Acad. Sci.*, 808:116–124.
- Kolláth, Z., Buchler, J. R., Serre, T. and Mattei, J. (1998). Analysis of the Irregular Pulsations of AC Herculis. *Astron. Astrophys.*, 329:147–155.
- Letellier C. & Gouesbet, G. (1997). Topological Structure of Chaotic Systems *Ann. N.Y. Acad. Sci.*, 808:51–78
- Letellier, C., Gouesbet, G., Soufi, F. *et al.* (1996). Chaos In Variable Stars : Topological Analysis of W Vir Model Pulsations. *Chaos*, 6(3):466–476.
- Ott, E. (1993). *Chaos in Dynamical Systems* (Univ. Press: Cambridge).
- Press, W. H., Teukolski, S. A., Vetterling, W. T. *et al.* (1992). *Numerical Recipes* (University Press: Cambridge).
- Sauer, T., Yorke, J. A. and Casdagli, M. (1991). Embedology. *J. Stat. Phys.*, 65:579–616.
- Serre, T. and Nesme-Ribes E. 1997, *The Evolution of the Solar Cycle*, – in *International School of Physics "Enrico Fermi", Course CXXXIII, Past and Present Variability of the Solar-Terrestrial System: Measurement, Data Analysis and Theoretical Models*, Eds. G. Cini Castagnoli & A. Provenzale, Societ Italiana de Fisica, Bologna, Italy. pp. 291–309.
- Serre, T. and Nesme-Ribes E. 2000, Nonlinear Analysis of Solar Cycles, *Astronomy & Astrophysics* (in press)
- Serre, T., Kolláth, Z. and Buchler, J. R., (1996a). Search For Low-Dimensional Nonlinear Behavior in Irregular Variable Stars – The

- Global Flow Reconstruction Method. *Astron. Astrophys.*, 311:833–844. [SKB96]
- Serre, T., Kolláth, Z. & Buchler, J. R., (1996b). Search For Low-Dimensional Nonlinear Behavior in Irregular Variable Stars – The Analysis of W Vir Model Pulsations. *Astron. Astrophys.*, 311:845–851.
- Thompson, J. M. T. and Stewart H. B. (1986). *Nonlinear Dynamics and Chaos* (New York: Wiley).
- Weigend, A.S & Gershenfeld, N. A. (1994). *Time Series Prediction* (Addison-Wesley: Reading).
- Wigner, J. (1932). On the quantum correction for thermodynamic equilibrium. *Phys. Rev.*, 40:749–759